# Quantum Effects in Ge and Si. I

J. J. STICKLER, H. J. ZEIGER, AND G. S. HELLER
*Lincoln Laboratory,* Massachusetts Institute of Technology, Lexington, Massachusetts*
(Received March 30, 1962; and in final form July 16, 1962)

Experimental quantum effect spectra have been observed in germanium and silicon at liquid helium temperatures and a frequency of 136 kMc/sec. Detailed spectra are presented for the applied magnetic field in the [100], [111], and [110] directions. Anisotropy data of some of the more intense lines are also presented. Using the theory of Luttinger and Kohn with the assumption of thermal equilibrium, effective masses and line intensities were computed for an applied magnetic field in the [111] direction. By adjusting the parameters of the theory, good agreement was obtained between the theoretical and experimental spectra. The experimentally determined parameters are:

| | $\gamma_1$ | $\gamma_2$ | $\gamma_3$ | $\kappa$ |
|---|---|---|---|---|
| Ge | 13.2 | 4.10 | 5.62 | 3.29 |
| Si | 4.22 | 0.50 | 1.35 | −0.39 |

These lead to parameters $A=13.2$, $|B|=8.2$, and $|C|=13.3$ for germanium and $A=4.22$, $|B|=1.0$, and $|C|=4.34$ for silicon. (See note added in proof.)

## 1. INTRODUCTION

IT has been pointed out by Luttinger and Kohn[1] and Luttinger[2] that deviations from the classical cyclotron resonance of holes in germanium and silicon should occur for transitions between levels of low quantum number. According to these theories, the energy-level spacing at high quantum numbers becomes uniform and the allowed transition frequencies approach the usual classical light and heavy hole cyclotron resonance frequencies. However, at low quantum numbers the degeneracy of the valence bands at $k=0$ becomes important and gives rise to nonuniformly spaced levels and hence a number of allowed transitions whose frequencies differ from the classical cyclotron resonance frequencies. These nonclassical resonance lines have been referred to as quantum effects. Goodman[3] and Evtuhov[4] have discussed the theory of quantum effects in some detail.

In order to observe quantum effects, it is necessary that a significant fraction of holes be in states of low quantum number at the applied magnetic field for resonance. This condition may be achieved if $\eta=\hbar\omega/kT \gtrsim 1$, where $\omega$ is the angular frequency at which the experiment is performed and $T$ is the absolute temperature of the holes in the valence bands. Quantum effects were first observed in germanium by Fletcher[5] at 24 kMc/sec and 1.2°K, corresponding to $\eta\approx 0.8$. Because he was so close to the threshold for observation of the quantum effects, Fletcher had to exercise great care to avoid heating of the carriers. Goodman[3] has tentatively interpreted these observations using the Luttinger theory. More recently, Hensel[6] has reported observations in germanium at 56 kMc/sec and 1.2°K; and Stickler *et al.*[7] have obtained spectra in germanium at 1.2°K and silicon at 4.2°K, both at a frequency of 136 kMc/sec.

An analysis of the data obtained by Stickler *et al.* has been made in germanium and silicon for the case where the magnetic field is along the [111] direction. Computer calculations have been made of the energy levels and the line intensities at thermal equilibrium for the most intense lines. In Sec. 2 of this paper, the experimental procedure is discussed and the results presented. The theory is discussed in Sec. 3. In Sec. 4, the analysis of the experiments is presented, and in Sec. 5 the results are discussed and compared with previous classical analyses.[8–10] The analysis of the data in the [100] and [110] directions will be the subject of a future paper.

## 2. EXPERIMENTAL PROCEDURE

The measurements were made in a 2-mm cavity spectrometer operating at a frequency of 136.6 kMc/sec. Most of the measurements were made using frequency doubling from a 4-mm klystron. Some of the later ones were made using a 2-mm CSF carcinotron as the source.

Figure 1 shows the block diagram of the system. The klystron was a Philips DX–151 which had an output power of about 100 mW at 68.3 kMc/sec. Power from the klystron passed through a 4-mm isolator to a point contact crystal harmonic generator using a silicon,

* Operated with support from the U. S. Army, Navy, and Air Force.

[1] J. M. Luttinger and W. Kohn, Phys. Rev. **97**, 869 (1955).
[2] J. M. Luttinger, Phys. Rev. **102**, 1030 (1956).
[3] R. R. Goodman, Phys. Rev. **122**, 397 (1961).
[4] V. Evtuhov, Phys. Rev. **125**, 1869 (1962).
[5] R. C. Fletcher, W. A. Yaeger, and F. R. Merritt, Phys. Rev. **100**, 747 (1955).
[6] J. C. Hensel, Bull. Am. Phys. Soc. **6**, 115 (1961).
[7] J. J. Stickler, C. Rauch, H. J. Zeiger, and G. S. Heller, Bull. Am. Phys. Soc. **6**, 115 (1961).
[8] R. N. Dexter, H. J. Zeiger, and B. Lax, Phys. Rev. **95**, 557 (1954).
[9] G. Dresselhaus, A. F. Kip, and C. Kittel, Phys. Rev. **98**, 368 (1955).
[10] R. N. Dexter, H. J. Zeiger, and B. Lax, Phys. Rev. **104**, 637 (1956).

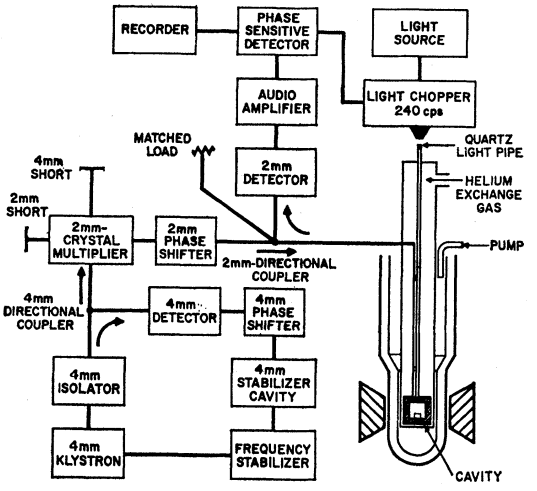


FIG. 1. Block diagram of 2-mm cavity spectrometer.

ion-bombarded crystal as the multiplying element.[11] The multiplier had a conversion efficiency of about 23 dB when tuned for maximum output. The 2-mm output of the multiplier was transmitted through a 2-mm waveguide to a 3-dB, 2-mm directional coupler of the hybrid ring type.[12] A phase shifter inserted between the directional coupler and multiplier served to match the multiplier to the rest of the microwave transmission line. The power was transmitted to the sample cavity through thin-walled silver-plated stainless-steel waveguide. An oversized waveguide was used to minimize the loss of the millimeter energy in the long waveguide section to the cavity.

The cylindrical cavity operated in the $TM_{016}$ mode with the sample placed on the bottom end wall in the region of maximum electric field as shown in Fig. 2. The sample was a thin disk whose faces were (110) planes. The microwave electric field was essentially normal to the plane of the disk. Carriers were optically excited in the sample by shining light through a quartz rod, the end of which was inserted through a hole in the top wall of the cavity. The hole diameter was small enough so that it was beyond cutoff at 2 mm with the quartz rod inserted. Tuning of the cavity was accomplished by varying the depth of insertion of the quartz rod into the cavity.

The experiment was performed in a conventional glass helium, nitrogen double Dewar system. The cavity and the portion of waveguide and light pipe within the Dewar were contained in a vacuum-tight stainless-steel tube containing a low pressure of helium gas for heat exchange. This eliminated noise which

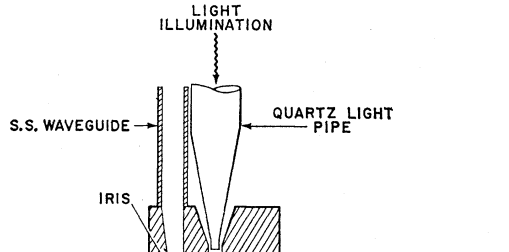


FIG. 2. Details of $TM_{016}$ spectrometer sample cavity.

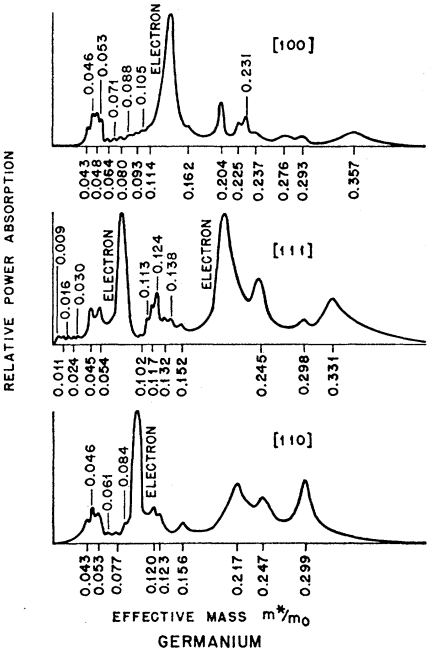


FIG. 3. Composite reproduction of recorder traces showing intensity of absorption in Ge vs applied magnetic field in the [100], [111], and [110] directions at 1.2°K, 136 kMc/sec. The effective masses of the quantum lines are indicated.

arises from bubbling of helium liquid in the sample cavity and waveguide. The exchange gas pressure could be regulated to control the temperature of the sample. The temperature of the cavity was monitored by a carbon resistance thermometer attached to the outside bottom of the cavity.

The Dewar system was placed between the pole faces of an electromagnet which could be rotated in the horizontal plane so that a uniform magnetic field could be applied to the sample in any direction in the (110) plane. The maximum field that could be achieved with this magnet was 19 kG, which corresponds to an effective mass of 0.39 at 136.6 kMc/sec.

The signal reflected from the cavity was monitored by a detector on one of the ports of the directional

[11] R. S. Ohl, P. P. Budenstein, and C. A. Burrus, Rev. Sci. Instr. **30**, 765 (1959).

[12] C. G. Montgomery, *Techniques of Microwave Measurement, Radiation Laboratory Series* (McGraw-Hill Book Company, Inc., New York, 1947), Vol. 11.

coupler. The modulation signal produced by chopping the light to the sample at 240 cps was amplified, phase detected, and displayed on a recorder trace as the magnetic field was swept.

The 2-mm signal was frequency stabilized by locking the 4-mm source to a high-$Q$ external, tunable 4-mm cavity. The 4-mm power was frequency modulated at 2000 cps. Some of the 4-mm power from the source was sampled through a directional coupler, then passed through a phase shifter to the high-$Q$ cavity. (See Fig. 1.) An in-guide crystal detector inserted between the coupler and phase shifter monitored the stabilization signal. The phase shifter was adjusted to produce a symmetrical cavity absorption dip as seen at the detector. The signal at the detector, resulting from the frequency modulation, was synchronously detected and

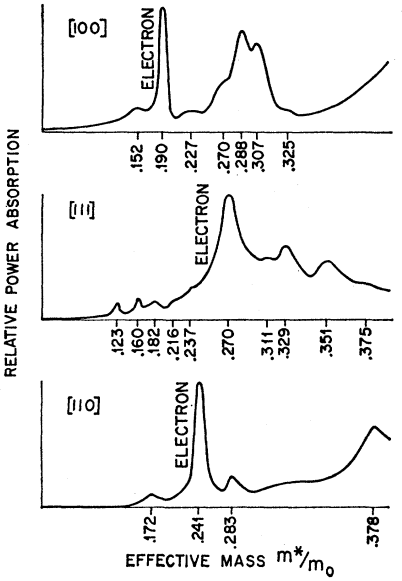


FIG. 4. Composite reproduction of recorder traces showing intensity of absorption in Si vs applied magnetic field in the [100], [111], and [110] directions at 4.2°K, in 136 kMc/sec. The effective masses of the quantum lines are indicated.

fed back to the klystron supply to stabilize frequency in the usual manner.

Most of the observations on germanium were made at 1.2°K, where relatively noise free spectra were obtained. At this temperature the value of the parameter $\eta$ was $\approx 6$. In the case of silicon, however, lowering the temperature below 4.2°K reduced the photoconductivity to such an extent that it was impossible to make observations. At 4.2°K, the value of $\eta$ was $\approx 1.8$ which still satisfied the condition for the observation of quantum effects.

For germanium, the light and millimeter power were lowered to the point where further reduction made no significant change in the spectrum. In the case of silicon, it was difficult to lower light and millimeter power to achieve this condition without the deterioration of the

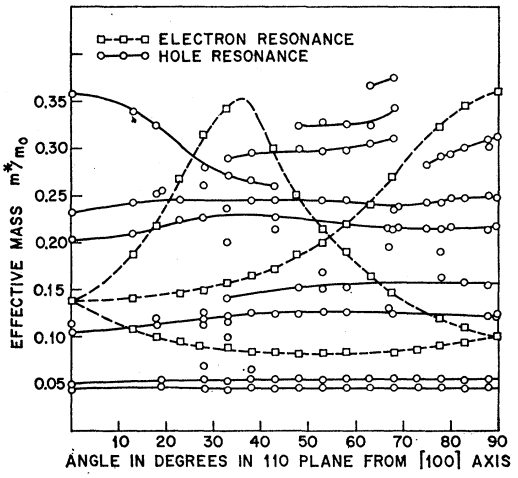


FIG. 5. Anisotropy of several of the quantum lines in Ge. Discontinuities occur because of the interference of the strong electron resonances.

signal-to-noise ratio. For example, with the applied magnetic field along the [111] direction, when the light intensity was lowered to the point where most of the quantum effect lines disappeared into the noise, a new line appeared at an effective mass of 0.123 (Fig. 4). This indicated that the carriers in silicon were not quite at the temperature of the lattice at excitation levels necessary to observe the quantum effect spectra.

Figures 3 and 4 show the observed spectra for germanium and silicon, respectively, for the magnetic field along the [100], [111], and the [110] directions. The anisotropy of some lines which could be followed are shown in Figs. 5 and 6. Some of the lines could not be followed continuously because of the interference of the strong electron lines.

### 3. THEORY OF ANALYSIS

The analysis of the experimental results was made on the basis of the theory of Luttinger.[2] The valence band

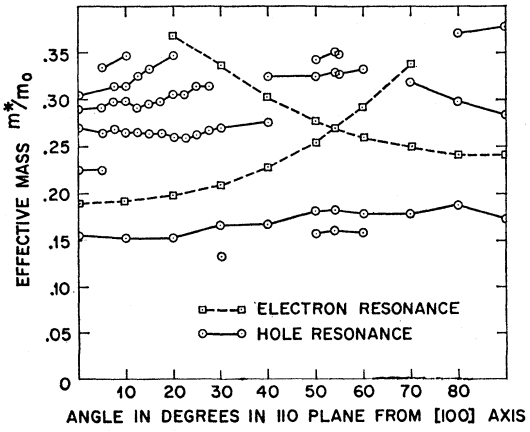


FIG. 6. Anisotropy of several of the quantum lines in Si. Discontinuities occur because of the interference of the strong electron resonances.

maxima in Ge and Si occur at the center of the Brillouin zone. In the absence of spin-orbit interaction, the band edges are sixfold degenerate, including spin. The spin-orbit interaction partially lifts this degeneracy, lowering two levels by an amount $\lambda$ with respect to the remaining four degenerate levels. In Ge, $\lambda\sim 0.29$ eV,[13] and in Si, $\lambda\sim 0.035$ eV.[14] At the temperatures at which cyclotron resonance of holes is usually observed, the energies of the holes in the fourfold degenerate bands are so low that the effect of the lower pair of bands can be neglected. In this case, Luttinger has shown that the most general set of effective mass equations for the fourfold set in the presence of a uniform magnetic field, and consistent with the symmetry of the lattice, is

$$D\psi=\mathcal{E}\psi, \tag{1}$$

where $D$ is of the form

$$\begin{aligned}D=&-(1/m)\{(\gamma_1+\tfrac{5}{2}\gamma_2)P^2/2\\&-\gamma_2(P_x^2J_x^2+P_y^2J_y^2+P_z^2J_z^2)\\&-2\gamma_3(\{P_xP_y\}\{J_xJ_y\}+\{P_yP_z\}\{J_yJ_z\}\\&+\{P_zP_x\}\{J_zJ_x\})+(e\hbar/c)\kappa\mathbf{J}\cdot\mathbf{H}\\&+(e\hbar/c)q(J_x^3H_x+J_y^3H_y+J_z^3H_z)\},\end{aligned} \tag{2}$$

for $x$, $y$, and $z$ along the crystal cube axes. Here $P_x=(\hbar/i)\partial/\partial x+(e/c)A_x$, etc., and $m$ is the free electron mass. The symbol $\{P_xP_y\}$ means $\frac{1}{2}(P_xP_y+P_yP_x)$. The $J_x$, $J_y$, $J_z$ are $4\times4$ angular momentum matrices for the case $J=\frac{3}{2}$. These are given by Luttinger. The wave function $\psi$ is a four element column wave function. The parameter $q$ is probably quite small for Ge and Si, and will be neglected.[2]

Luttinger has shown that the problem takes the simplest form for $\mathbf{H}$ along a [111] direction. For that reason, the present first analysis was carried out for this case only. Goodman[15] has given the transformation of $D$ to a coordinate system with $z$ axis (or axis 3), along a [111] direction. When $\mathbf{H}$ is taken along [111] and the operators $P_1$, $P_2$, $P_3$ in the new coordinate system are replaced by

$$\begin{aligned}a^\dagger&=(c/2\hbar eH)^{\frac{1}{2}}\quad(P_1+iP_2),\\a&=(c/2\hbar eH)^{\frac{1}{2}}\quad(P_1-iP_2),\\P_H&=(c/\hbar eH)^{\frac{1}{2}}\quad P_3,\end{aligned} \tag{3}$$

the matrix $D$ becomes

$$\begin{aligned}D=&-(\hbar eH/mc)\\&\times\begin{pmatrix}(\gamma_1+\gamma_3)(a^\dagger a+\frac{1}{2})+\frac{3}{2}\kappa+\frac{1}{2}(\gamma_1-2\gamma_3)P_H^2 & -(\frac{1}{3})^{\frac{1}{2}}[(\gamma_2+2\gamma_3)a^{\dagger2}+2(\gamma_3-\gamma_2)a^\dagger P_H] & -(\frac{2}{3})^{\frac{1}{2}}[(\gamma_3-\gamma_2)a^{\dagger2}+(\gamma_3+2\gamma_2)a^\dagger P_H] & 0\\ -(\frac{1}{3})^{\frac{1}{2}}[(\gamma_2+2\gamma_3)a^{\dagger2}+2(\gamma_3-\gamma_2)aP_H] & (\gamma_1-\gamma_3)(a^\dagger a+\frac{1}{2})-\frac{1}{2}\kappa+\frac{1}{2}(\gamma_1+2\gamma_3)P_H^2 & 0 & (\frac{2}{3})^{\frac{1}{2}}[(\gamma_3-\gamma_2)a^{\dagger2}+(\gamma_3+2\gamma_2)aP_H]\\ -(\frac{2}{3})^{\frac{1}{2}}[(\gamma_3-\gamma_2)a^2+(\gamma_3+2\gamma_2)a^\dagger P_H] & 0 & (\gamma_1-\gamma_3)(a^\dagger a+\frac{1}{2})+\frac{1}{2}\kappa+\frac{1}{2}(\gamma_1+2\gamma_3)P_H^2 & -(\frac{1}{3})^{\frac{1}{2}}[(\gamma_2+2\gamma_3)a^{\dagger2}+2(\gamma_3-\gamma_2)a^\dagger P_H]\\ 0 & (\frac{2}{3})^{\frac{1}{2}}[(\gamma_3-\gamma_2)a^2+(\gamma_3+2\gamma_2)a^\dagger P_H] & -(\frac{1}{3})^{\frac{1}{2}}[(\gamma_2+2\gamma_3)a^{\dagger2}+2(\gamma_3-\gamma_2)aP_H] & (\gamma_1+\gamma_3)(a^\dagger a+\frac{1}{2})-\frac{3}{2}\kappa+\frac{1}{2}(\gamma_1-2\gamma_3)P_H^2\end{pmatrix}.\end{aligned} \tag{4}$$

The annihilation and creation operators $a$, $a^\dagger$ have the commutation relations, $[a,a^\dagger]=1$.

The solutions of Eq. (1) for $P_H=0$ are obtained by assuming the wave functions to be of the form

$$\psi_{n,\rho}=\begin{pmatrix}C_{n\rho}^1 & u_{n-2}\\ C_{n\rho}^2 & u_n\\ C_{n\rho}^3 & u_{n-4}\\ C_{n\rho}^4 & u_{n-2}\end{pmatrix}, \tag{5}$$

where $u_n$ is a harmonic oscillator wave function with the properties

$$\begin{aligned}au_n&=n^{\frac{1}{2}}u_{n-1},\\a^\dagger u_n&=(n+1)^{\frac{1}{2}}u_{n+1}.\end{aligned} \tag{6}$$

The subscript $\rho$ labels the four possible solutions of the $4\times4$ Schrödinger equation (1). For $n=0$, 1, $C_{n\rho}^1=C_{n\rho}^2=C_{n\rho}^3=0$; and for $n=2$, 3, $C_{n\rho}^3=0$. The energies, to second-order perturbation theory in $P_H$, are

$$\mathcal{E}_{n\rho}(P_H)=-(\hbar eH/mc)[\epsilon_{n\rho}+A_{n\rho}P_H^2]. \tag{7}$$

Here, $-(\hbar eH/mc)\epsilon_{n\rho}$ is the energy obtained from the solution of the problem for $P_H=0$, and

$$\begin{aligned}A_{n\rho}=&\tfrac{1}{2}\gamma_1+\gamma_3[|C_{n\rho}^2|^2+|C_{n\rho}^3|^2-|C_{n\rho}^1|^2-|C_{n\rho}^4|^2]\\&+\sum_{\rho'}\Big[(\tfrac{2}{3})^{\frac{1}{2}}(\gamma_3+2\gamma_2)\{(n+1)^{\frac{1}{2}}C_{n\rho}^2C_{n+3\rho'}^4-(n-1)^{\frac{1}{2}}C_{n\rho}^1C_{n+3\rho'}^3\}\\&\quad-\frac{2}{(3)^{\frac{1}{2}}}(\gamma_3-\gamma_2)\{(n+1)^{\frac{1}{2}}C_{n\rho}^2C_{n+3\rho'}^1+(n-1)^{\frac{1}{2}}C_{n\rho}^4C_{n+3\rho'}^3\}\Big]\Big/(\epsilon_{n\rho}-\epsilon_{n+3\rho'})\\&+\sum_{\rho'}\Big[(\tfrac{2}{3})^{\frac{1}{2}}(\gamma_3+2\gamma_2)\{(n-2)^{\frac{1}{2}}C_{n\rho}^4C_{n-3\rho'}^2-(n-4)^{\frac{1}{2}}C_{n\rho}^3C_{n-3\rho'}^1\}\\&\quad-\frac{2}{(3)^{\frac{1}{2}}}(\gamma_3-\gamma_2)\{(n-2)^{\frac{1}{2}}C_{n\rho}^1C_{n-3\rho'}^2+(n-4)^{\frac{1}{2}}C_{n\rho}^3C_{n-3\rho'}^4\}\Big]\Big/(\epsilon_{n\rho}-\epsilon_{n-3\rho'}).\end{aligned} \tag{8}$$

[13] A. H. Kahn, Phys. Rev. **97**, 1647 (1955).
[14] W. Kohn, *Solid State Physics*, edited by F. Seitz and D. Turnbull (Academic Press Inc., New York, 1957), Vol. 5.
[15] R. R. Goodman Ph.D. thesis, University of Michigan, 1958, (unpublished).

The effective mass for a transition between two levels, neglecting $P_H$ dependence, is

$$m^*(n\rho; n'\rho') = 1/|\epsilon_{n\rho} - \epsilon_{n'\rho'}|. \quad (9)$$

The perturbation giving electric dipole transitions due to a microwave electric field $\mathbf{E}$, is given by introducing a vector potential

$$\mathbf{A}' = (ic/\omega)\mathbf{E}.$$

The perturbation matrix is obtained by replacing $\mathbf{P}$ in (4) by $\mathbf{P}+(e/c)\mathbf{A}'$, and retaining terms first order in $\mathbf{E}$. The result is

$$D' = (e/2im\omega)(2\hbar eH/c)^{\frac{1}{2}} M(P_H), \quad (10)$$

where

$$M(P_H) = \begin{bmatrix} (\gamma_1+\gamma_3)(a^\dagger E^- + aE^+) + (\gamma_1-2\gamma_3)P_H E_3 & -(\frac{1}{3})^{\frac{1}{2}}[2(\gamma_2+2\gamma_3)aE^- + 2(\gamma_3-\gamma_2)(a^\dagger E_3 + P_H E^+)] & -(\frac{2}{3})^{\frac{1}{2}}[2(\gamma_3-\gamma_2)a^\dagger E^+ + (\gamma_3+2\gamma_2)(aE_3+P_H E^-)] & 0 \\ -(\frac{1}{3})^{\frac{1}{2}}[2(\gamma_2+2\gamma_3)a^\dagger E^+ + 2(\gamma_3-\gamma_2)(aE_3+P_H E^-)] & (\gamma_1-\gamma_3)(a^\dagger E^- + aE^+) + (\gamma_1+2\gamma_3)P_H E_3 & 0 & (\frac{2}{3})^{\frac{1}{2}}[2(\gamma_3-\gamma_2)a^\dagger E^+ + (\gamma_3+2\gamma_2)(aE_3+P_H E^-)] \\ -(\frac{2}{3})^{\frac{1}{2}}[2(\gamma_3-\gamma_2)aE^- + (\gamma_3+2\gamma_2)(a^\dagger E_3 + P_H E^+)] & 0 & (\gamma_1-\gamma_3)(a^\dagger E^- + aE^+) + (\gamma_1+2\gamma_3)P_H E_3 & -(\frac{1}{3})^{\frac{1}{2}}[2(\gamma_2+2\gamma_3)aE^- + 2(\gamma_3-\gamma_2)(a^\dagger E_3 + P_H E^+)] \\ 0 & (\frac{2}{3})^{\frac{1}{2}}[2(\gamma_3-\gamma_2)aE^- + (\gamma_3+2\gamma_2)(a^\dagger E_3 + P_H E^+)] & -(\frac{1}{3})^{\frac{1}{2}}[2(\gamma_2+2\gamma_3)a^\dagger E^+ + 2(\gamma_3-\gamma_2)(aE_3+P_H E^-)] & (\gamma_1+\gamma_3)(a^\dagger E^- + aE^+) + (\gamma_1-2\gamma_3)P_H E_3 \end{bmatrix} \quad (11)$$

and $E^+ = E_1 + iE_2$, $E^- = E_1 - iE_2$.

For the case $P_H = 0$, it is easy to see from (11) that the selection rule for $\mathbf{E}$ transverse to $\mathbf{H}$ is $\Delta n = \pm 1$; and the selection rule for $\mathbf{E}$ along $\mathbf{H}$ is $\Delta n = \pm 3$. Transitions $\Delta n = \pm 2, \pm 4$ are allowed only for $P_H \neq 0$. These selection rules are the quantum mechanical analogs of the classical result for fundamental and harmonic resonance with $\mathbf{H}$ along a [111] direction.[16] With the sample geometry of this experiment, $\mathbf{E}$ is essentially transverse to $\mathbf{H}$. However, a small longitudinal component of $\mathbf{E}$ may be introduced when the sample is placed in the cavity. We then expect that weak $\Delta n = \pm 3$ lines may appear, as well as $\Delta n = \pm 2, \pm 4$ lines introduced by the $P_H$ dependent terms of (11).

The peak intensity of a quantum effect resonance at thermal equilibrium should be proportional to

$$I(n\rho; n'\rho') \propto (H_{\rm res}) \times \frac{\int_{P_H} [e^{-\mathcal{E}_{n\rho}(P_H)/kT} - e^{-\mathcal{E}_{n'\rho'}(P_H)/kT}]}{\int_{P_H} \sum_{n''\rho''} e^{-\mathcal{E}_{n''\rho''}(P_H)/kT} dP_H} \times H_{\rm res} \times |M_{n\rho, n'\rho'}(P_H)|^2 dP_H \times \frac{1}{(\Delta H)_{\rm res}}. \quad (12)$$

The first factor on the right-hand side of (12) represents the proportionality of the density of Landau levels in a magnetic field to $H_{\rm res}$, the magnetic field for resonance. The second factor represents the population difference of the lower energy state $\mathcal{E}_{n\rho}(P_H)$ and the higher energy state $\mathcal{E}_{n'\rho'}(P_H)$ ($P_H$ is conserved in the transition). The factor $H_{\rm res} \times |M_{n\rho; n'\rho'}(P_H)|^2$ is proportional to the absolute value squared of the matrix element of the electric dipole interaction operator $D'$. The last factor is a measure of the breadth of the resonance line.

[16] H. J. Zeiger, B. Lax, and R. N. Dexter, Phys. Rev. **105**, 495 (1957).

This expression can be simplified in a number of ways. $H_{\rm res}$ can be eliminated by using the relation

$$\hbar\omega = (\hbar e H_{\rm res}/mc)(\epsilon_{n'\rho'} - \epsilon_{n\rho}).$$

We assume

$$(\Delta H)_{\rm res}/H_{\rm res} \sim 2/\omega\tau,$$

where $\tau$ is a characteristic relaxation time. We do not attempt in this paper to calculate the intensities of $\Delta n = \pm 2, \pm 4$ transitions. For this reason, the dependence of $M(P_H)$ on $P_H$ will be neglected. Finally, the integration over $P_H$ in the population factor can be performed. Combining these steps, and retaining only relevant factors, the expression we take for the intensity is

$$I(n\rho; n'\rho') = \frac{|M_{n\rho, n'\rho'}|^2}{|\epsilon_{n\rho} - \epsilon_{n'\rho'}|} \times \frac{1 - \left(\frac{A_{n\rho}}{A_{n'\rho'}}\right)^{\frac{1}{2}} \exp(-\eta)}{\sum_{n''\rho''} \left(\frac{A_{n\rho}}{A_{n''\rho''}}\right)^{\frac{1}{2}} \exp\left(-\eta \frac{\epsilon_{n''\rho''} - \epsilon_{n\rho}}{|\epsilon_{n\rho} - \epsilon_{n'\rho'}|}\right)}, \quad (13)$$

where $\eta = \hbar\omega/kT$.

## 4. ANALYSIS OF EXPERIMENTAL RESULTS

To analyze the experimental results for $\mathbf{H}$ along the [111] direction, a possible set of parameters $\gamma_1, \gamma_2, \gamma_3, \kappa$ was chosen, based on the analysis of classical cyclotron resonance.[10] These parameters, along with the appropriate value of $\eta$, were then substituted into the expressions for $m^*(n\rho; n'\rho')$ and $I(n\rho; n'\rho')$, and a machine calculation was performed.

The analysis of classical cyclotron resonance is not sufficient to determine the sign of $\gamma_2$ and $\gamma_3$ uniquely, and gives no direct information on $\kappa$. However, theo-

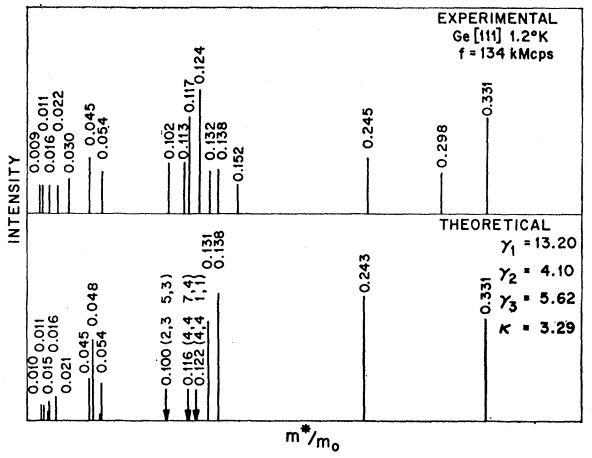


FIG. 7. Comparison of experimental and theoretical spectra for Ge in the [111] direction. The lines indicated by arrows correspond to possible higher order transitions.

retical considerations[9] indicate that the only ambiguity between physically reasonable choices is in the sign of $\gamma_2$ for Si. Furthermore, the band structure of Ge and Si indicate that the band structure parameter[9] $H_2$ for both should be small, and if $H_2$ is zero, then an exact relation exists between $\kappa$ and $\gamma_1, \gamma_2, \gamma_3$:

$$\kappa=(3\gamma_3+2\gamma_2-\gamma_1-2)/3. \tag{14}$$

We therefore chose a reasonable set of parameters $\gamma_1, \gamma_2, \gamma_3$, and assumed as a starting point that (14) held, thus determining $\kappa$. When the intensities of lines vs their effective mass were plotted, the theoretical and experimental patterns showed enough similarity that a reasonable identification of lines could be made. This would have been difficult without the intensity calculation, since the theoretical masses were not always very close to the experimental. (However, see note added in proof.) Once the identification of transitions was established, it was possible to adjust the values of $\gamma_1$, $\gamma_2$, $\gamma_3$ (still assuming $H_2=0$), to improve the fit. When a few prominent lines were adjusted to give the most reasonable fit, many other theoretical lines fell into place with respect to the observed spectra. It was then found that a number of experimental lines could be reasonably explained as $\Delta n=\pm 2$, or $\pm 3$ transitions from low-lying levels to excited states. For both Ge and Si, the assumption $H_2=0$ gave a rather good fit of the data within the experimental error, so that it was never necessary to relax this condition.

Figure 7 shows a comparison of the theoretical and experimental spectrum for the best fit of effective masses in Ge. It can be seen that the theoretical intensities for $\Delta n=\pm 1$ transitions are in reasonably good agreement with experiment. There are no lines of significant intensity in the theoretical spectrum which are not found in the experimental spectrum. However, there are several lines in the experiment which do not appear in the theoretical spectrum. The best values of the parameters $\gamma_1$, $\gamma_2$, $\gamma_3$, $\kappa$ obtained for Ge, along with the values of other parameters derived from these are given in Table I. These parameters are very close to those obtained by Goodman.[3] Figure 8 shows the strong transitions identified in this experiment.

TABLE I. Valence band parameters of Ge and Si.

| | Ge | Si |
|---|---|---|
| $\gamma_1$ | 13.2 | 4.22 |
| $\gamma_2$ | 4.10 | 0.50 |
| $\gamma_3$ | 5.62 | 1.35 |
| $\kappa$ | 3.29 | −0.39 |
| $F$ | −28.7 | −5.00 |
| $G$ | −0.95 | −1.11 |
| $H_1$ | −6.0 | −4.22 |
| $H_2$ | ~0 | ~0 |
| $L$ | −30.6 | −7.22 |
| $M$ | −6.0 | −4.22 |
| $N$ | −33.7 | −8.10 |
| $A$ | 13.2 | 4.22 |
| $\lvert B\rvert$ | 8.2 | 1.0 |
| $\lvert C\rvert$ | 13.3 | 4.34 |
| $(m_L^*)_{[111]}$ | 0.042 | 0.151 |
| $(m_H^*)_{[111]}$ | 0.379 | 0.547 |

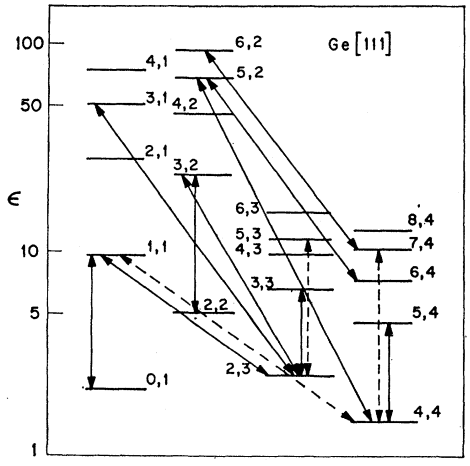


FIG. 8. Strong transitions which have been identified in the spectrum of Ge in the [111] direction. The dotted lines represent possible higher order transitions.

Figure 9 shows the best fit of the theoretical spectrum to the experiment for Si. In this case, the experimental accuracy (~5%) was not as good as for Ge. All the experimental lines observed in the case of Si could be reasonably accounted for. There are a number of lines which should be observed at fields higher than we have available at present. The intensity fit is not as good as for Ge. There is experimental evidence, discussed in Sec. 3, that carrier heating effects are important in Si.

The best values of the parameters obtained for Si are $\gamma_1=4.22$, $\gamma_2=0.50$, $\gamma_3=1.35$, $\kappa=-0.39$. We were not able to find a reasonable fit of the experimental data starting with the other physically reasonable choice,

$\gamma_1 \cong 4$, $\gamma_2 \cong -0.5$, $\gamma_3 \cong 1.3$. Table I gives the parameters derived from our values of $\gamma_1$, $\gamma_2$, $\gamma_3$, and $\kappa$. These disagree with a set of values obtained theoretically.[17] Figure 10 shows the transitions observed in the experiment.

## 5. DISCUSSION

The parameters, $A$, $B$, $C$, that we obtain for Ge and Si agree with those obtained from analysis of the classical cyclotron resonance results within the errors quoted for these experiments.[9,10] (See note added in proof.) There are a number of possible explanations of the extra lines observed in the case of Ge. Among these are, (1) carriers in other bands (the line at $m^*=0.030$ may,

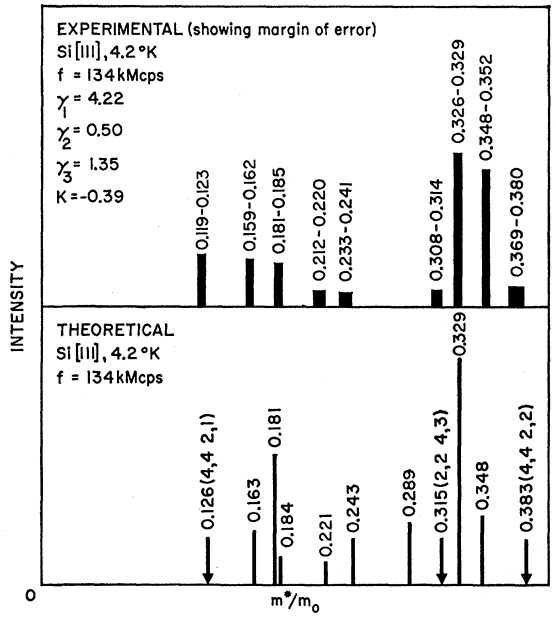


FIG. 9. Comparison of experimental and theoretical spectra for Si in the [111] direction. The lines indicated by arrows correspond to possible higher order transitions, whose intensities have not been computed. The width of the lines in the experimental spectrum represent the error in the determination of the effective mass value. The theoretical line at 0.289 is obscured by a strong electron line.

for example, be the $\mathbf{k}=0$ electron); (2) carriers associated with the spherical pockets at the ends of the constant energy surface along [111] axes. This latter possibility is being examined theoretically.

There are indications in both Ge and Si, that carrier heating may be playing some role in affecting populations, and therefore line intensities. Carrier heating is proportional to the acoustical phonon scattering time, which is proportional to an elastic constant, and inversely proportional to a deformation potential squared.[18] Recent experiments on cyclotron resonance of holes in

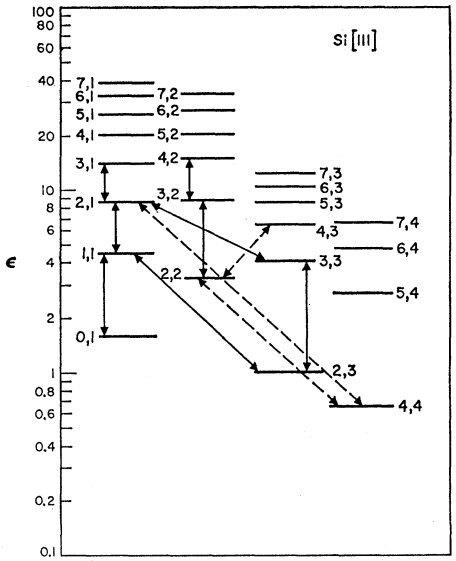


FIG. 10. Strong transitions which have been identified in the spectrum of Si in the [111] direction. The dotted lines represent possible higher order transitions.

diamond[19] seem completely interpretable classically, even though for those experiments $\eta \sim 3$. The elastic constants of diamond are quite large,[20] and this fact combined with small valence band deformation potentials could explain the apparent carrier heating in diamond.

We plan to use the values of the parameters obtained for the [111] case, to compute effective masses and line intensities for the [100] and [110] cases. We also plan to carry out machine computations of the intensities of $P_H$-induced, $\Delta n=\pm 2$ transitions.

*Note added in proof.* An abstract of this paper, published earlier, quoted different values of the parameters for Ge. Our earlier analysis was based on the identification of the line at $m^*=0.124$ in the Ge [111] spectrum as a $\Delta n=\pm 1$ transition in the theoretical spectrum. By an unfortunate coincidence, this allowed the weak experimental line at $m^*=0.298$ to be identified as a $\Delta n=\pm 2$ transition, adding strength to this interpretation.

Subsequent experiments in a cavity configuration which suppressed any leakage of $E \| H$, eliminated the line at $m^*=0.124$, identifying this line as $\Delta n=\pm 3$ transition, and forcing the new interpretation of the data given in this paper.

We wish to thank Dr. W. Mercouroff of the University of Paris for re-emphasizing the discrepancy between the parameters in the earlier abstract, and experimental observations in the classical limit. We also wish to thank him for sending us values of the Ge parameters from his thesis (University of Paris, June 1962), with which our new parameters agree fairly closely.

[17] L. Kleinman and J. C. Phillips, Phys. Rev. **118**, 1153 (1960).
[18] J. M. Ziman, *Electrons and Phonons* (Clarendon Press, Oxford, 1960), p. 433.
[19] C. Rauch, Phys. Rev. Letters **7**, 83 (1961), and (private communication).
[20] C. Kittel, *Introduction to Solid State Physics* (John Wiley & Sons, Inc., New York, 1956), 2nd ed., p. 93.

ACKNOWLEDGMENTS

The authors would like to thank R. S. Ohl and C. A. Burrus of the Bell Telephone Laboratories for providing the ion-bombarded silicon used in the multipliers and for many helpful discussions concerning multiplier design. Discussions of the theory with L. Roth and G. Dresselhaus proved very profitable. Thanks are due to C. Rauch for his participation in the early phases of the experiments. The authors would further like to thank J. B. Thaxter for the design of some of the millimeter components and Richard Koch for invaluable assistance throughout the entire experiment. Aid in programming the computations of effective masses and line intensities by Virginia Mason is greatly appreciated. Finally, the authors are greatly indebted to G. W. Catuna for his extensive work in adjusting the theoretical spectra to fit the experimental results.

PHYSICAL REVIEW VOLUME 127, NUMBER 4 AUGUST 15, 1962

# Amplification of Acoustic Waves through Interaction with Conduction Electrons

HAROLD N. SPECTOR*
*Department of Physics, The Hebrew University, Jerusalem, Israel*
(Received April 12, 1962)

It is shown, from a Boltzmann equation treatment, that in the presence of a dc electric field it is possible for an acoustic wave to gain energy from the conduction electrons in a material. The criterion for such an amplification of an acoustic wave to take place is that the drift velocity given to the conduction electrons in the direction of propagation by the dc field must exceed the velocity of sound. In metals, dc fields of such a magnitude cannot be maintained, but in semiconductors the necessary conditions can be satisfied and an amplification of the acoustic wave can take place.

## I. INTRODUCTION

In the past few years, much work, both theoretical[1–5] and experimental[6–8] has been done on the absorption of ultrasonic waves via an interaction with the conduction electrons in metals, semimetals, and semiconductors. However, only recently was it discovered by Hutson, McFee, and White[9] that amplification of ultrasonic waves occurred in CdS via the same interaction in the presence of a dc field. Weinreich has shown, using a phenomenological treatment,[10] that when there is a dc electric field which gives the conduction electrons a drift velocity the direction of propagation greater than in the velocity of sound, the wave is amplified instead of absorbed. It has been pointed out, however, that the phenomenological approach is only valid when the sound wavelength is longer than the mean free path, i.e., $ql<1$. A more general approach must be made through the use of the Boltzmann equation.[4] Since the electronic contribution to the absorption of ultrasound in materials at low temperatures can be quite large when $ql>1$, it is, therefore, of interest to examine the whole problem of the electron-acoustic wave interaction in the presence of a dc electric field using the Boltzmann equation treatment.

In Sec. II, we will use the model of a free electron gas developed by Cohen, Harrison, and Harrison for the conduction electrons in a metal[2] and, in general, adopt the formalism developed by them. This model has also been used for semimetals[3] and semiconductors.[5] In Secs. III and IV we shall consider the cases of the dc field parallel and transverse to the direction of propagation, respectively. In Sec. V we give a discussion of the results of our calculations.

## II. CONSTITUTIVE EQUATION

The conduction electrons are replaced by the model of a free electron gas of density $N_0$. The sound wave of wave number $q$ and frequency $\omega$ manifests itself as a velocity field $\mathbf{u}(\mathbf{r},t)\propto\exp[i(qz-\omega t)]$ in the positive background which has the same density as the electron gas. The interaction between the acoustic wave and the electrons can be represented partly through the means of a self-consistent internal electromagnetic field and partly by means of a deformation potential. The self-consistent electromagnetic field induced by the passage of the sound wave is derived from Maxwell's equations. In our case, the latter can be written in the form

$$\mathbf{J}_1+N_0e\mathbf{u}=-\sigma_0\mathbf{B}\cdot\boldsymbol{\mathcal{E}}, \tag{2.1}$$

* National Science Foundation Postdoctoral Fellow.
[1] A. B. Pippard, Phil. Mag. **46**, 1104 (1955); Proc. Roy. Soc. (London) **A257**, 165 (1960).
[2] M. H. Cohen, M. J. Harrison, and W. A. Harrison, Phys. Rev. **117**, 937 (1960).
[3] M. J. Harrison, Phys. Rev. **119**, 1260 (1960).
[4] N. Mikoshiba, J. Phys. Soc. Japan **15**, 982 (1960).
[5] H. N. Spector, Phys. Rev. **125**, 1192 (1962).
[6] H. E. Bömmel, Phys. Rev. **96**, 220 (1954); L. Mackinnon, Phys. Rev. **98**, 1181 (1955).
[7] R. W. Morse, H. V. Bohm, and J. D. Gavenda, Phys. Rev. **109**, 1394 (1958); T. Olson, Phys. Rev. **118**, 1007 (1960).
[8] D. H. Reneker, Phys. Rev. **115**, 303 (1959).
[9] A. R. Hutson, J. H. McFee, and D. L. White, Phys. Rev. Letters **7**, 237 (1961).
[10] G. Weinreich, Phys. Rev. **104**, 321 (1956).